Microchimica Acta (2022) 189:122
https://doi.org/10.1007/s00604-022-05233-5

ORIGINAL PAPER

# Hydrophobic laser-induced graphene potentiometric ion-selective electrodes for nitrate sensing

**Robert G. Hjort[1] · Raquel R. A. Soares[1] · Jingzhe Li[2,3] · Dapeng Jing[4] · Lindsey Hartfiel[5] · Bolin Chen[1] · Bryan Van Belle[1] · Michelle Soupir[5] · Emily Smith[2,3] · Eric McLamore[6] · Jonathan C. Claussen[1] · Carmen L. Gomes[1]**

Received: 12 July 2021 / Accepted: 15 February 2022


## Abstract

Current solid-contact ion-selective electrodes (ISEs) suffer from signal-to-noise drift and short lifespans partly due to water uptake and the development of an aqueous layer between the transducer and ion-selective membrane. To address these challenges, we report on a nitrate ISE based on hydrophobic laser-induced graphene (LIG) coated with a poly(vinyl) chloride–based nitrate selective membrane. The hydrophobic LIG was created using a polyimide substrate and a double lasing process under ambient conditions (air at 23.0 ± 1.0 °C) that resulted in a static water contact angle of 135.5 ± 0.7° (mean ± standard deviation) in wettability testing. The LIG–ISE displayed a Nernstian response of − 58.17 ± 4.21 mV $dec^{-1}$ and a limit-of-detection (LOD) of 6.01 ± 1.44 µM. Constant current chronopotentiometry and a water layer test were used to evaluate the potential (emf) signal stability with similar performance to previously published work with graphene-based ISEs. Using a portable potentiostat, the sensor displayed comparable ($p > 0.05$) results to a US Environmental Protection Agency (EPA)–accepted analytical method when analyzing water samples collected from two lakes in Ames, IA. The sensors were stored in surface water samples for 5 weeks and displayed nonsignificant difference in performance (LOD and sensitivity). These results, combined with a rapid and low-cost fabrication technique, make the development of hydrophobic LIG–ISEs appealing for a wide range of long-term in situ surface water quality applications.

**Keywords** Ion-selective electrodes (ISE) · Solid contact · PVC membrane · Graphene · Potentiometry · Water quality · Agricultural nutrients

✉ Carmen L. Gomes
carmen@iastate.edu

Robert G. Hjort
ghjort@iastate.edu

Raquel R. A. Soares
raquel20@iastate.edu

Jingzhe Li
jzli@iastate.edu

Dapeng Jing
djing@iastate.edu

Lindsey Hartfiel
lmurry@iastate.edu

Bolin Chen
bolin@iastate.edu

Bryan Van Belle
brynvnbl@iastate.edu

Michelle Soupir
msoupir@iastate.edu

Emily Smith
esmith1@iastate.edu

Eric McLamore
emclamo@clemson.edu

Jonathan C. Claussen
jcclauss@iastate.edu

[1] Department of Mechanical Engineering, Iowa State University, Ames, IA 50011, USA

[2] Department of Chemistry, Iowa State University, Ames, IA 50011, USA

[3] The Ames Laboratory, U.S. Department of Energy, Ames, IA 50011, USA

[4] Materials Analysis and Research Laboratory, Iowa State University, Ames, IA 50011, USA

[5] Department of Agricultural and Biological Engineering, Iowa State University, Ames, IA 50011, USA

[6] Agricultural Sciences Department, Clemson University, Clemson, SC 29634, USA

Published online: 26 February 2022

## Introduction

Ion-selective electrodes (ISEs), which convert ionic activity to electric potential (emf), are a common non-destructive method for ion detection in a wide range of industries. The pH meter, a selective glass electrode to the hydrogen ion ($H^+$), is an early example of an ISE [1]. Researchers soon expanded beyond pH monitoring with the advent of selective membrane ISEs [2], and by the late 1960s, several were available for various ions [3]. However, the use of a liquid junction in these ISEs limited their applications due to high maintenance and complications with miniaturization [4]. Solid-contact ISEs remove the inner liquid solutions allowing the ion-selective membrane to make direct contact with the transducing layer. The first example of a solid-contact ISE was the coated-wire electrode (CWE) [5]. Early CWEs had a simple design but possessed a problem with emf drift due to thermodynamically ill-defined ("blocked") interfaces, formation of oxygen half-cells, and/or the presence of a thin water layer between the electrode and ion-selective membrane [4, 6]. These issues with CWEs led to significant research into solid-contact ISEs including various conducting polymers [7, 8] and nanomaterials [9].

Nanostructured conducting allotropes of carbon have proven a promising material for energy and sensing applications due to their mechanical strength, electrochemical properties, and inert nature [10]. Carbon materials such as carbon nanotubes [11], graphene [12], and graphene oxide [13] have been applied as solid contacts for ISEs. Graphene in particular is highly conductive with high mechanical strength that provides an excellent platform for sensing and biosensing [14]. In 2014, Lin et al. [15] first reported on a method to produce a 3D graphitic-like structure commonly referred to as laser-induced graphene (LIG). In this procedure, the $sp^3$-carbon atoms in polyimide (PI, Kapton) are photothermally converted to $sp^2$-carbon by a $CO_2$ infrared laser ($\lambda = 10.6$ μm) producing a black porous 3D structure [16]. Further research has demonstrated the ability to form similar material with various lasers [17] and on carbon precursors such as cloth, paper, and food [18]. This maskless, direct writing, one-lasing process eliminates the need for annealing procedures and/or precious metal deposition commonly used on graphene produced through ink-jet printing [19], aerosol-jet printing [20], and chemical vapor deposition (CVD) [21] methods to improve the electrical conductivity and electrocatalytic nature. LIG has become a popular substrate for sensing purpose due to its rapid and scalable production method and has been applied towards electrochemically sensing a variety of analytes including pathogens [22] and various molecules and proteins [23–26]. Ion sensing with LIG was first demonstrated by Garland et al. [27] in soil columns with the goal of deploying these in farm fields for fertilizer monitoring ($NO_3^-$ and $NH_4^+$). Results from this study show a rapid Nernstian response, and recoveries in soil of 96% and 95% for ammonium and nitrate, respectively. LIG has also been applied to sensing ions in urine [28] ($K^+$ and $NH_4^+$). Both potassium and ammonium LIG–ISEs accurately assessed hydration levels in real urine samples and displayed a shelf-life of up to 3 months under dry storage. Recently, LIG was utilized for multi-analyte sensing in sweat including potentiometrically monitoring ions ($K^+$) [29]. This study also reported using LIG as a pseudo reference electrode with electrochemically deposited Ag/AgCl; however, due to influence of $Cl^-$ ions on the pseudo reference electrode, results show a super-Nernstian sensitivity of 95 mV $dec^{-1}$ for potassium. These previous studies have demonstrated the feasibility of LIG (fabricated via one-lasing process) as a transducer for ISEs; however, detailed fabrication of the LIG for this particular function is still lacking, and in particular, studies focused on developing hydrophobic LIG–ISEs for long-term environmental monitoring and the possible pitfalls associated with it (e.g., signal drift and sensor longevity) are still needed.

Herein, we report on a nitrate ISE using hydrophobic LIG fabricated by a double lasing process under ambient conditions (air at $23.0 \pm 1.0$ °C). A $CO_2$ laser and PI film were used to create the hydrophobic LIG in a direct writing process without the need for extraneous reagents, post-fabrication annealing processes, or catalyst deposition. This LIG fabrication technique circumvents the need to perform additional chemical modification or lasing in an inert gas environment, demonstrating a more scalable method to create hydrophobic LIG than previous reports. Material characterizations show a 3D porous structure dominated by $sp^2$-carbon with Raman spectra showing typical D, G, and 2D peaks of LIG. Wettability testing was performed with five liquids, and a modified Zisman plot was created to estimate the critical surface tension of the hydrophobic LIG. A PVC–based nitrate selective membrane that uses the quaternary ammonium salt tridodecylmethylammonium nitrate (TDMAN) was drop-casted onto the LIG to form a solid-contact at the interface. The hydrophobic LIG–ISE was calibrated using open circuit potentiometry (OCP) and was subjected to selectivity tests, stability characterization, and sensing nitrate in environmental water samples from two lakes in Ames, IA with comparable performance to a US Environmental Protection Agency (EPA)–accepted method. The results obtained in this study demonstrate the potential hydrophobic LIG–ISEs have for long-term in situ monitoring of ions in surface waters.

## Materials and methods

All ion-selective membrane chemicals, potassium ferro/ferricyanide, sodium nitrite, and sodium sulfate were purchased from Millipore Sigma (Darmstadt, Germany). Sodium nitrate, sodium chloride, and sodium bicarbonate were purchased from Thermo Fisher Scientific (MA, USA). Commercial polyimide (PI) film with 5-m thickness was purchased from McMaster-Carr (OH, USA).

### Laser-induced graphene fabrication

Hydrophobic LIG electrodes were designed in CorelDraw (Corel Corporation, Canada) and fabricated with a 75-W M2 Fusion Epilog $CO_2$ laser (Epilog Laser, CO, USA). The first lasing (i.e., hydrophilic LIG) was performed at 15% speed and 7% power followed immediately by a secondary lasing (i.e., hydrophobic LIG) at 20% speed and 3% power. Both laser treatments were performed in air (23.0 ± 1.0 °C) with a + 1-mm offset from the laser focal point and a total lens to material distance of ~ 41 mm at 1200 DPI. The working area of the electrodes (diameter of 5 mm) was separated from the connection point with a fast-drying lacquer. Contacts of the LIG–ISE were protected with a conductive silver ink (Cl-1001, Engineering Materials Systems Inc., OH, USA). After fabrication, the LIG electrodes were briefly rinsed with ethanol and dried under nitrogen gas. The nitrate-selective membrane was prepared by mixing 1.5 wt% tridodecylmethylammonium nitrate (TDMAN), 0.5 wt% methyltriphenylphosphonium bromide, 5.75 wt% polyvinyl chloride (PVC), 16.25 wt% 2-nitrophenyl octyl ether (2-NPOE), and 76 wt% THF for a total mass of 1000 mg. After vortex mixing for ~ 1 min and sonicating for ~ 3 min, two applications of 10 µL was drop-casted onto the freshly fabricated LIG and allowed to dry overnight in a vacuum desiccator. The hydrophobic LIG–ISEs were then conditioned in 1 mM $NaNO_3$ for 24 h prior to calibration.

### Surface characterization

X-ray photoelectron spectroscopy (XPS) measurements were performed using a Kratos Amicus/ESCA 3400 instrument. The samples were irradiated with 240 W unmonochromated Mg $K_\alpha$ X-rays. Photoelectrons emitted at 0° from the surface normal were energy-analyzed using a DuPont type analyzer. The pass energy was set at 150 eV and a Shirley baseline was removed from all reported spectra. CasaXPS was used to process raw datafiles. Scanning electron microscopy (SEM) analysis was carried out using a FEI Quanta 250 field emission microscope and an accelerating voltage of 10 kV. The samples were coated with 2 nm of iridium to enhance conductivity.

Raman measurements were performed by a Horiba XploRA Plus confocal Raman microscope. A 532-nm laser operating at 1.2 mW and a 50 × objective (0.5 NA) was used to check the LIG with 30 s acquisition time and 3 accumulations. Raman spectra at 12 random locations on the LIG were collected. All Raman peaks were fitted to a Lorentzian function in Igor Pro 6.37. The $I_D/I_G$ and $I_{2D}/I_G$ ratios were calculated from the fitting results.

A ramé-hart model 90 goniometer equipped with an automated dispensing system (ramé-hart p/n 100–22, ramé-hart instrument co., Succasunna, NJ) was used for all static contact angle measurements using a 3-µL droplet. Images were generated and analyzed using DROPimage Pro software where the contact angle was estimated. The wettability of the hydrophobic LIG was tested using five solvents (DI water, methanol, dimethyl sulfoxide (DMSO), formamide, and glycerol (Sigma-Aldrich)). The static contact angles were plotted versus the surface energy of each liquid to create a modified Zisman plot used to estimate the critical surface tension ($\gamma_c$) of the hydrophobic LIG.

### Electrochemical characterization and nitrate sensing

Constant current chronopotentiometry, cyclic voltammetry (CV), and electrochemical impedance spectroscopy (EIS) measurements were performed on a CH Instruments electrochemical analyzer (model CHI7018E, CH Instruments Inc., TX, USA). Open-circuit potentiometry (OCP) for calibration, selectivity testing, water layer testing, temperature and pH sensitivity, and surface water analysis was performed on a PalmSens 4 potentiostat (PalmSens, Netherlands) equipped with a MUX8-R2 multiplexer. Hydrophobic LIG working electrodes and an external Ag/AgCl electrode (3 M KCl liquid junction) were the reference electrode for all experiments. For chronopotentiometry, CV, and EIS analysis, a platinum wire electrode (99.95% Pt, 0.5 mm dia.) functioned as the counter electrode.

The LIG–ISE was calibrated from $10^{-7}$ to $10^{-1}$ by 0.5 log steps in DI water under agitation from a small magnetic stir bar (200 rpm) using stock solutions of $NaNO_3$ added by pipette. Activities were calculated with the extended Debye-Hückel equation (Eq. S3). Selectivity testing was performed using the fixed-interference method (FIM) [30] for four interfering ions ($NO_2^-$, $Cl^-$, $HCO_3^-$, and $SO_4^{2-}$) and a constant concentration of 1 mM while varying the nitrate concentrations. The selectivity coefficients were calculated using Eq. S5.

CV and EIS analyses of the bare hydrophobic LIG were performed with 5-mM ferro/ferricyanide in 0.1-M KCl. CV scans were performed from − 0.4 to 0.6 V at five scan rates

from 10 to 200 mV $s^{-1}$. EIS frequency range was 1 MHz to 1 Hz with an AC amplitude of 0.2 V and a DC voltage of 0 V. After drop casting the ion-selective membrane, EIS spectra were collected with unconditioned, 24-h conditioned, and 72-h conditioned hydrophobic LIG–ISEs (all in 0.1 M $NaNO_3$) using the above parameters.

### Water layer and chronopotentiometry

The potential stability of the ion-selective membrane and hydrophobic LIG substrate interface was studied using constant current chronopotentiometry and a water layer test [31]. For chronopotentiometry measurements, the LIG–ISEs were conditioned in 0.1 M $NaNO_3$ for 24 h followed by applying a ± 1 nA current for 60 s each while recording the emf signal. For the water layer test, LIG–ISEs were conditioned in 10 mM NaNO3 for 24 h followed by monitoring the emf signal for 5 h in $NaNO_3$, then 10 mM NaCl for 5 h, and finally 10 mM $NaNO_3$ for 14 h. Electrodes were briefly rinsed with DI water in between transfers.

### Temperature and pH sensitivity

Temperature influence on the sensitivity of the LIG–ISEs was studied at three temperatures (23.0, 30.0, and 45.0 ± 1.0 °C) controlled by a hot plate and monitored with a glass thermometer (± 0.5 °C accuracy). The pH influence was tested at two nitrate concentration levels (1 mM and 100 mM) using National Institute of Standards and Technology (NIST) pH buffer solutions of 5.02, 7.00, 8.95, and 10.01 pH (Thermo Fisher Scientific, MA, USA).

### Surface water analysis and sensor longevity

Samples from two local lakes in Ames, IA were collected, stored at 2–8 °C, and tested within 48 h of collection. For potentiometric ion measurements, US EPA method 9210a was followed. Potentiometric ion sensing results were confirmed by a secondary laboratory with a combined nitrate and nitrite detection Seal Analytical AQ2 method (EPA-114A Rev. 11) where nitrite levels were measured (EPA-116A Rev. 5) and subtracted from the combined measurement results to estimate nitrate concentration.

The LIG–ISEs were submerged in collected water samples for 5 weeks and tested weekly to monitor the change in LOD and sensitivity over time. The samples were stored in ambient lab conditions and sensors were calibrated in whole log steps from $10^{-6}$ to $10^{-2}$ with similar conditions as stated above. Cross sectional SEM images were obtained of fresh LIG–ISEs and those stored in water samples to visually compare the effect on membrane adhesion.

### Data analysis

All measurements were made in triplicate and were reported as mean ± standard deviation. Data analysis was performed using MATLAB (R2020a, The MathWorks Inc., Natick, MA). Mean response signals from the linear portion of the calibration curve were used to determine the sensitivity and the limit-of-detection (LOD) was calculated using the 3 $\sigma$ method. The response time was calculated as the time required to reach 95% of the steady-state signal (t95). One-way analysis of variance (ANOVA) and Student's *t*-test were performed with JMP Pro v.15 statistical software (SAS Institute, Cary, NC) using a significance level of 0.05. All figures were generated in SigmaPlot 14 (Systat Software Inc., San Jose, CA).

## Results and discussion

### Surface characterization

The XPS analysis showed that LIG samples after second laser treatment (Fig. 1e) are mainly consisted of $sp^2$-cabon evidenced by the asymmetric main peak at 284.0 eV and the broad $\pi - \pi^*$ peak at 290.0 eV. The $sp^3$ type hydrocarbon and oxidized carbon are also present on the surface shown by the symmetric, slightly broader peaks ranging from 285.0 to 288.0 eV. Assuming that the carbon content of the polyimide film is 50–60% [32], it is likely that the other bonds (i.e., H, N, and O) were broken by the high temperatures and released as gasses [16]. XPS analysis after the second laser treatment of the PI film resulted in 92.8% carbon.

Raman spectra of the hydrophobic LIG (Fig. 1f) displayed prominent D, G, and 2D bands, which are typical for LIG [15]. The D band (~ 1339 $cm^{-1}$) originates from graphene lattice defect sites, the G band (~ 1579 $cm^{-1}$) arises from in-plane vibrations of sp2-carbon atoms and is present in all graphitic material, and the 2D band or G' band (~ 2682 $cm^{-1}$) originates from a two-phonon double resonance process [33]. The $I_D/I_G$ ratio was calculated as 1.1 ± 0.1, which indicates high disorder in the LIG structure [34]. Additionally, the $I_{2D}/I_G$ ratio was calculated as 0.5 ± 0.03 indicating a multilayer graphitic-like structure [35]. The Raman results were spatially uniform over different sampling locations. (see Table S1 for more details.)

A sufficiently hydrophobic surface is one method of preventing an aqueous layer from developing between the interface of the solid-contact transducing layer and ion-selective membrane [36]. The hydrophobic LIG in this study displayed a static contact angle of 135.5 ± 0.7° for DI water. The static contact angle was measured for five solvents and results are shown in Fig. 2. If these measurements are plotted against the surface energy of each liquid, a modified

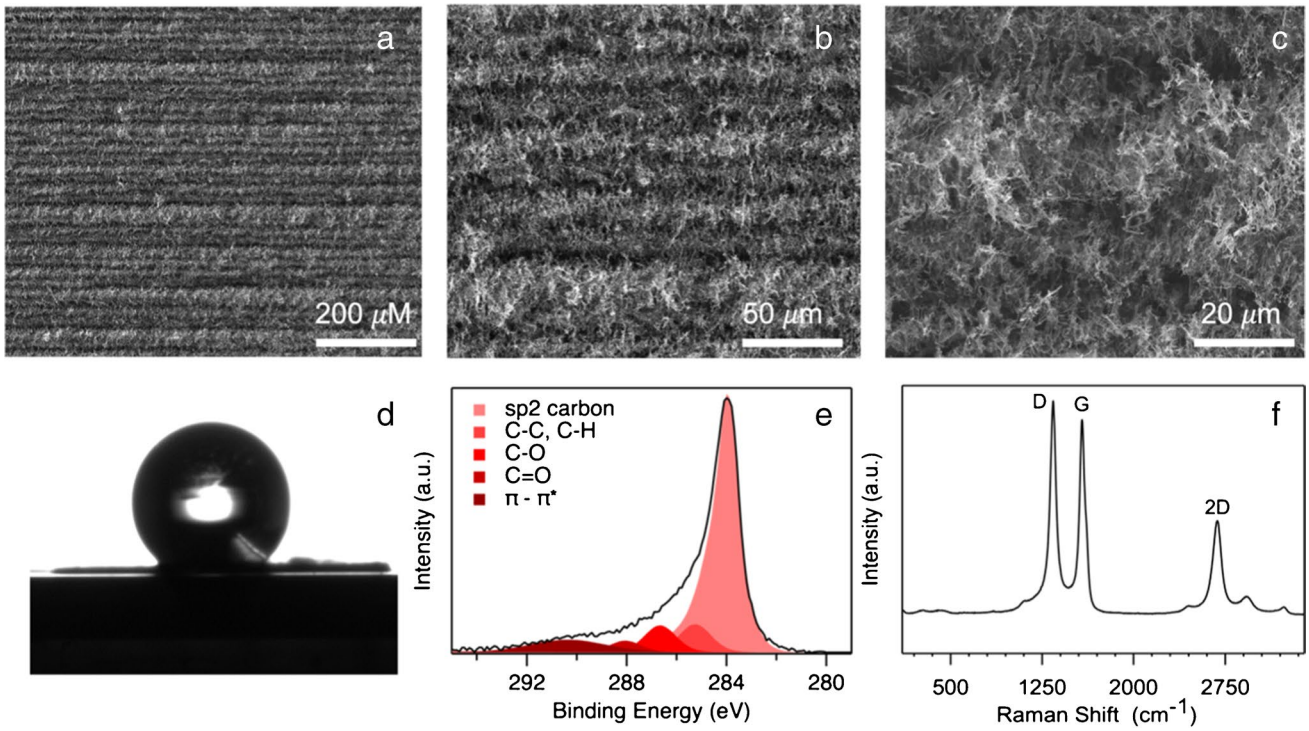


**Fig. 1** **a**, **b**, and **c** SEM image after second laser treatment showing the rough flattened hydrophobic LIG. **d** Static contact angle photograph of DI water displaying the hydrophobic nature of the LIG. **e** XPS spectra showing predominately $sp^2$-carbon. **f** Average Raman spectra displaying the typical D, G, and 2D peaks of LIG

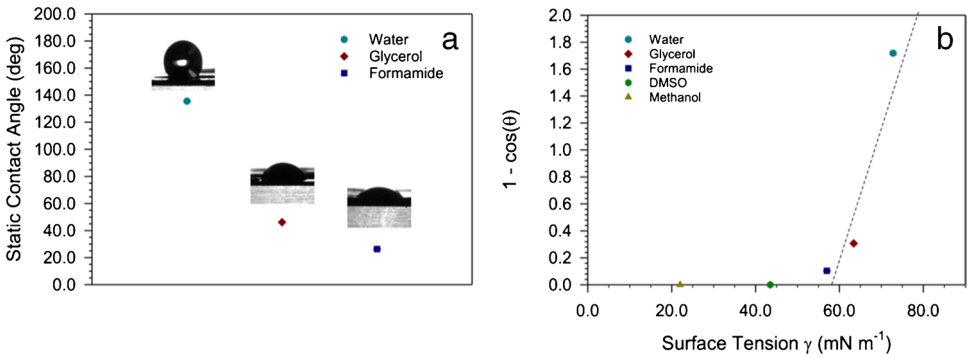


**Fig. 2** **a** Static contact angle measurements and corresponding photographs of water (135.5 ± 0.7°), glycerol (46.1 ± 0.3°), and formamide (26.3 ± 0.5°) droplets. **b** Modified Zisman plot used to estimate the critical surface tension ($\gamma_c$) of the hydrophobic LIG at the intersection of the linear regression line and the x-axis. $\gamma_c$ was estimated as 57.7 ± 0.08 mN $m^{-1}$. Data represents mean ± standard deviation ($n = 3$)

Zisman plot (Fig. 2b) can be used to estimate the critical surface tension ($\gamma_c$) of the hydrophobic LIG by fitting a model using linear regression analysis and extrapolating to the intersection with the x-axis [37]. This value can then be used to quickly assume the behavior of a given liquid on the LIG surface. If $\gamma < \gamma_c$, then the liquid should wet the LIG surface and vice versa for $\gamma > \gamma_c$ [38]. For the hydrophobic LIG, $\gamma_c$ was estimated as 57.7 ± 0.03 mN $m^{-1}$ suggesting that water (72.75 mN $m^{-1}$) [39] should not wet the surface and methanol (22.95 mN $m^{-1}$) [39] should, as experimental results confirm.

## Nitrate calibration and selectivity

Open circuit potentiometry (OCP) was used to create calibration curves for the nitrate sensors in DI water by sequentially increasing the nitrate concentration in the electrochemical cell (Fig. 3 and Fig. S5). The slope of the linear portion

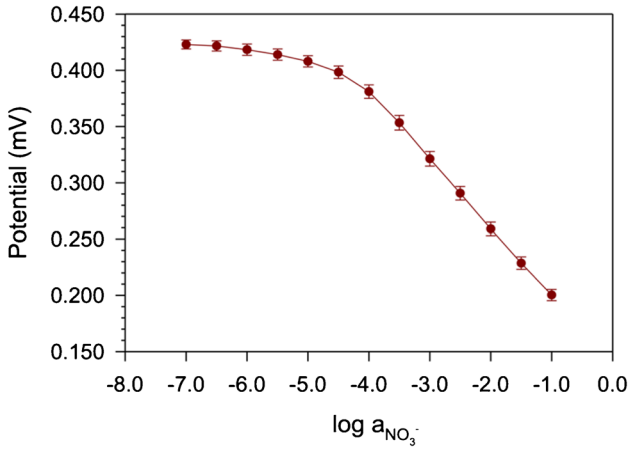


**Fig. 3** Calibration curve for $NO_3^-$. The average sensitivity was $-58.17 \pm 4.21$ mV $dec^{-1}$ and LOD was $6.01 \pm 1.44$ µM with a response time (t95) of $12.52 \pm 3.28$ s. Data represents mean ± standard deviation ($n = 3$)

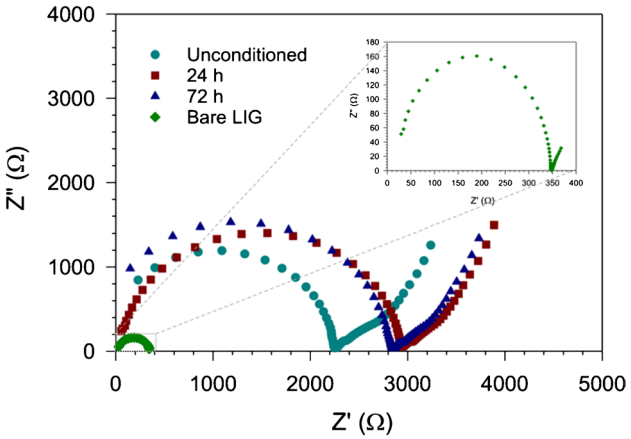


**Fig. 4** Representative EIS spectra of unconditioned, 24-h conditioned, and 72-h conditioned hydrophobic LIG–ISEs in 0.1 M $NaNO_3$ with a nonsignificant difference between the 24- and 72-h conditioned LIG–ISEs. Inset shows a representative EIS spectra of bare hydrophobic LIG in 5-mM ferri/ferrocyanide in 0.1-M KCl with an $R_{ct}$ of $0.291 \pm 0.057$ k Ω

of the calibration curve was reported as the sensitivity using the average value of the steady-state signal for each concentration. According to the Nernst equation, at 25 °C for a monovalent anion, the sensitivity for an ISE is − 59.16 mV $dec^{-1}$ [40]. For the hydrophobic LIG–ISEs, the average sensitivity was $-58.17 \pm 4.21$ mV $dec^{-1}$. The slight sub-Nernstian response is possibly due to incomplete membrane conditioning or the diffusion of small molecules (e.g., $H_2O$, $CO_2$, $O_2$) across the polymeric ion-selective membrane [41]. The LOD ($3\sigma$) was calculated as $6.01 \pm 1.44$ µM and the linear range was ~ $10^{-3.5}$ to $10^{-1}$ M with a response time (t95) of $12.52 \pm 3.28$ s. A slight improvement in sensitivity and LOD is demonstrated here with the hydrophobic LIG relative to other LIG–based nitrate ISEs [27]; however, the LOD is higher than nitrate ISEs based on conducting polymers or organosulfur compounds such as tetrathiafulvalene (TTF) with similar emf signal drift (see Table S3 for more information). This is likely due to the larger bulk capacitance and smaller resistance of the hydrophobic LIG as compared to the slightly hydrophilic LIG produced from a diode laser ($\lambda = 405$nm) [42].

The fixed interference method (FIM), with a constant interfering ion concentration of 1 mM, was used for all interference testing. The selectivity coefficients (Table 1) are similar to previously reported work intended for agricultural applications [43, 44] with $Cl^-$ and $NO_2^-$ showing the largest interference. $NO_2^-$ is typically not present at large concentrations in surface waters due to multiple rapid oxidation pathways [45] and may not be a cause for concern. However, the presence of $Cl^-$ can create challenges for nitrate ISEs especially intended for environmental monitoring. In areas with high concentrations of $Cl^-$ ions, desalination techniques [46] may need to be implemented to accurately estimate nitrate levels in situ.

**Table 1** Selectivity coefficients ($logK^{POT}_{NO_3^-,j}$) at 1 mM interfering ion concentration. Values given are mean ± standard deviations ($n = 3$)

| Ion, $j$ | $logK^{POT}_{NO_3^-,j}$ |
|---|---|
| $Cl^-$ | $-1.70 \pm 0.09$ |
| $NO_2^-$ | $-1.61 \pm 0.05$ |
| $HCO_3^-$ | $-2.93 \pm 0.08$ |
| $SO_4^{2-}$ | $-2.43 \pm 0.16$ |

## Electrochemical impedance spectroscopy and cyclic voltammetry

EIS analysis of ISEs has been proposed to determine physical damage, biofouling, and leaching of membrane components offering a simple and rapid way to characterize ISE functionality in situ [47]. This is particularly beneficial for ISEs for wide usage in, possibly remote, environmental settings where issues with physical damaging and biofouling are prevalent. EIS has also been used to show the water uptake of polymeric ion-selective membranes [48]. The high water uptake of PVC–based is a drawback that can lead to water layer formation, emf signal instability, and membrane delamination [49]. Samples of unconditioned, 24-h conditioned, and 72-h conditioned LIG–ISEs were used to evaluate the water uptake during conditioning of the electrodes. Figure 4 shows the resulting EIS spectra and the change in bulk resistance from unconditioned ISEs ($2.222 \pm 0.028$ $k\Omega$) to conditioned ($3.254 \pm 0.363$ $k\Omega$ for 24 h, $3.208 \pm 0.323$ $k\Omega$ for 72 h). The inset shows the bare hydrophobic LIG charge transfer resistance ($R_{ct}$, $0.291 \pm 0.057$ $k\Omega$). A nonsignificant ($p = 0.8778$) change is shown between the 24- and

72-h conditioning step. These results are somewhat expected based on in-depth studies of water uptake by polymeric membranes showing uptake beginning only after 10 min upon contact with the aqueous solutions with the majority occurring in the first 10 h [50]. CV analysis of bare hydrophobic LIG (Fig. S4) displays quasi-reversible behavior with a peak separation of 167.0 ± 9.5 mV at 10 mV $s^{-1}$ and an electroactive surface area (ESA) of 0.278 ± 0.038 $cm^2$. The ESA is approximately 70% larger than the geometric area (0.196 $cm^2$) and is likely due to the unordered porous nature of LIG, allowing for more exposure of edge plane sites to the redox solution [51].

## Water layer test and chronopotentiometry

The water layer test (or aqueous layer test) proposed by Fibbioli et al. [31] has become a common validation step in the development of solid-contact ISEs. Results from this test can help determine if a truly solid contact has formed between the ion-selective membrane and the underlying transducer. The formation of an inner water layer can develop upon contact with the aqueous sample, and conditions of the fabrication process (e.g., humidity) have also shown to influence the possibility of an aqueous layer to develop [41]. When a water layer forms, ISEs will experience long equilibration times, substantial emf signal drift, and/or sensitivity to $CO_2$ partial pressure. Over time, the later can continue to spread over the interface affecting the adhesion of the membrane and ultimately lead to delamination. For this study, LIG–ISEs were conditioned for 24 h in 10 mM $NaNO_3$, followed by monitoring the emf for 5 h. The electrodes were then transferred to 10 mM NaCl for 5 h, and finally back to 10 mM $NaNO_3$ for 14 h, all while monitoring the emf signal. Figure 5 shows the resulting time versus emf response with a drift upon return to the 10 mM $NaNO_3$ of 0.328 ± 0.040 mV $h^{-1}$. The initial jump when changing solutions is due to the change in phase boundary potential at the membrane/solution interface and is a function of the selectivity coefficient and the concentrations of the primary and interfering ions. The hydrophobic nature of the double lased LIG appears to hinder the development of a water layer and shows smaller drift relative to previously reported solid-contact nitrate ISEs intended for long-term use [52].

Potential stability of the emf response can also be influenced by the degree to which the solid contact can be polarized [53]. The small input current (typically < pA) from the high impedance voltmeter should have minimal effect for emf stability. As shown in Eq. S4, the emf signal drift is related to the capacitance of the solid contact where an increase in capacitance will lead to less drift in the emf response. This is particularly prudent when designing solid contact ISEs for continuous monitoring of ions

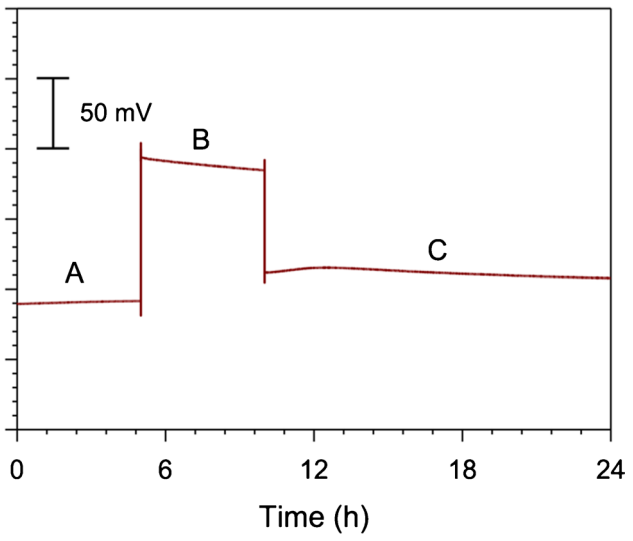


**Fig. 5** Representative 24-h water layer test. Solutions were 10 mM (A) $NaNO_3$, (B) NaCl, and (C) $NaNO_3$. The drift was 0.328 ± 0.040 mV $h^{-1}$ upon return to 10 mM $NaNO_3$

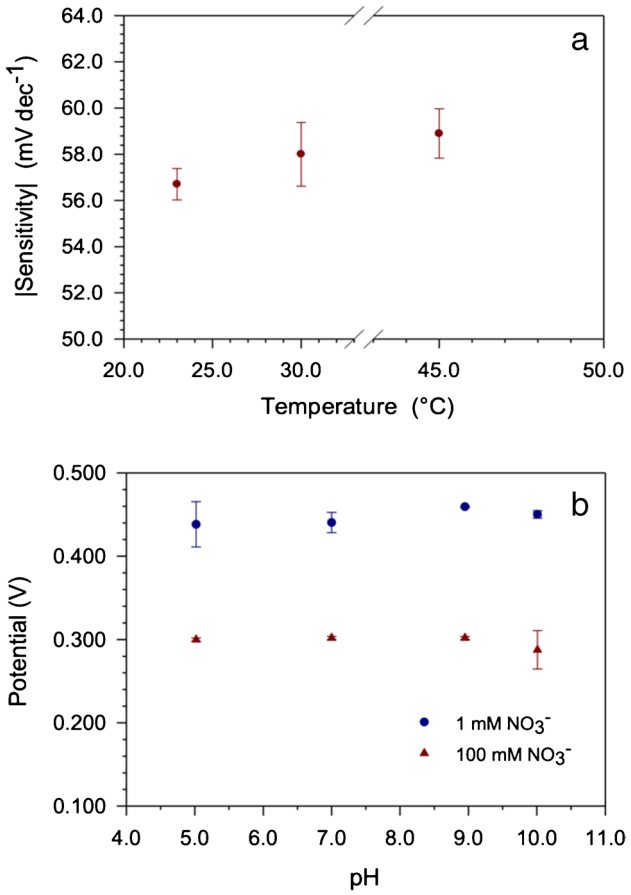


**Fig. 6** **a** Temperature effect on the sensitivity at 23.0, 30.0, and 45.0 ± 1.0 °C, showing a sensitivity dependance of 0.11 mV $°C^{-1}$. **b** Emf response at pH levels 5.02, 7.00, 8.98, and 10.01 showing a non-significant difference between responses at each concentration level. Data represents mean ± standard deviation ($n = 3$)

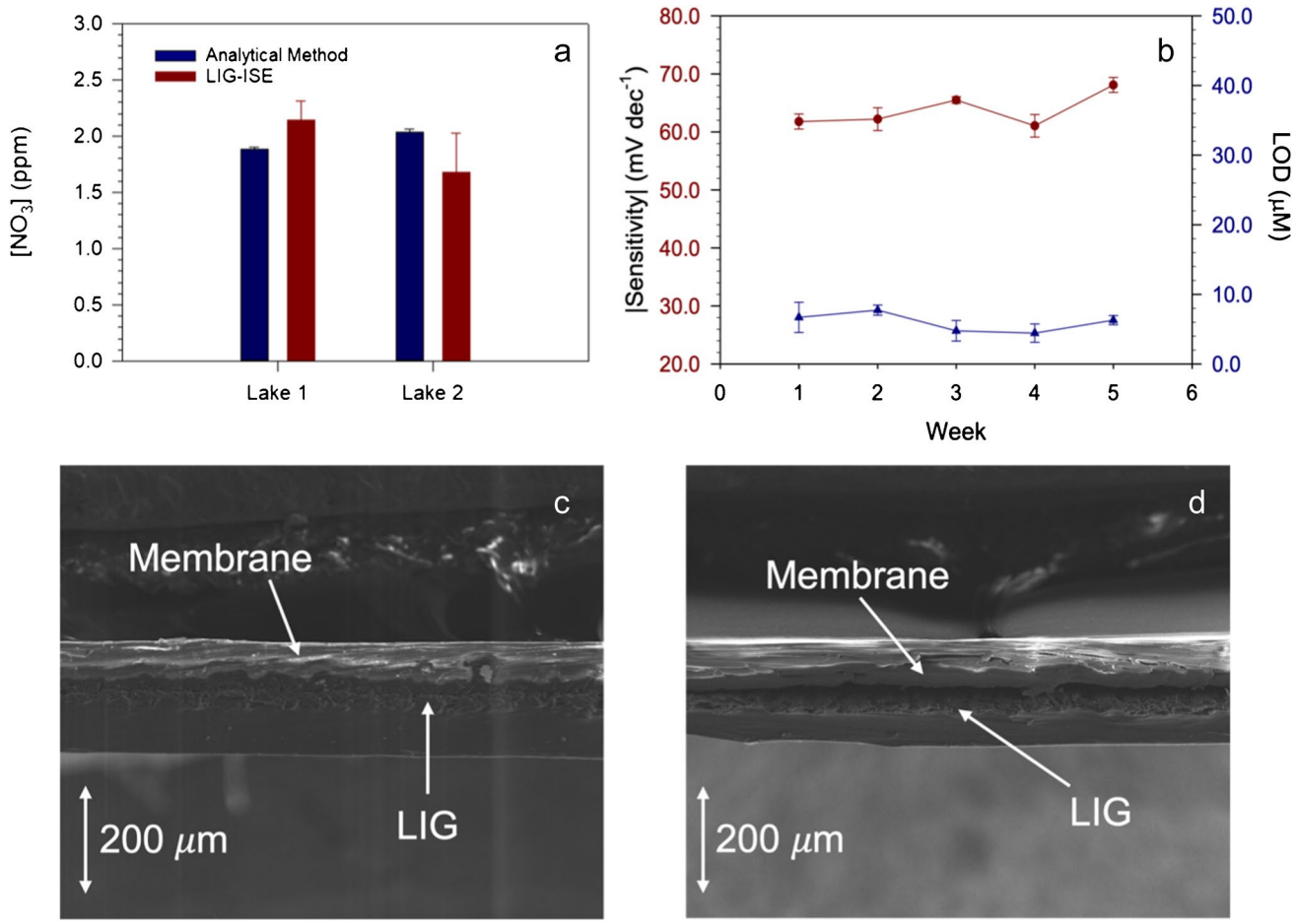


**Fig. 7** **a** Results from analysis of surface water from two lakes showing comparable ($p > 0.05$) performance between the analytical method (blue bars) and LIG–ISEs (red bars). **b** Sensitivity and LOD monitoring over 5 weeks of storage in surface water samples displaying minimal change ($p > 0.05$) over the 5 weeks. **c** SEM cross sectional image of an unconditioned LIG–ISE and **d** SEM cross sectional of an LIG–ISE after storage in surface water sample for 5 weeks showing the beginning of membrane delamination. Data represents mean ± standard deviation ($n = 3$)

over an extended period of time. Following Bobocka [54], which has become a common method in solid-contact ISE characterization, an applied current of ± 1 nA should be sufficient to polarize an electrode and evaluate the emf stability. For these tests, each current was applied for 60 s while recording the emf response (Fig. S6). The potential drift was 10.5 ± 0.96 μV $s^{-1}$ and the calculated capacitance was 95.24 ± 8.24 μF, which are similar to previously published work with graphene-based ISEs [13, 55]; however, it is much lower than other carbon-based solid contacts [56, 57]. Increasing the capacitance with conducting polymers or nanoparticles could further improve the emf stability of the LIG–ISEs and may have the added benefit of achieving E° reproducibility, eventually leading to calibration-free LIG–ISEs [58] and will be the focus of future work.

## Temperature and pH dependance

Calibration curves were performed at three different temperatures (23.0, 30.0, and 45.0 ± 1.0 °C) in DI water to evaluate the effects on the LIG–ISEs sensitivity (Fig. 6a). The increase of temperature resulted in a higher sensitivity which was expected as the Nernst equation has a positive linear dependance on temperature. Similar to previous works [59], the ion-selective membrane here has shown a temperature dependance of 0.11 mV $°C^{-1}$.

Ion-selective membranes can be affected by pH by altering the membrane charge leading to signal interference. Furthermore, gasses such as $CO_2$ can penetrate into developed water layers, causing change of the pH inside the layer and ultimately alter the emf signal [60]. Water pH is typically

within a narrow range, for example, river and ground water ranges from pH 6 to pH 8 [61]. The effect of pH was tested at two different nitrate levels (1 mM and 100 mM) in buffer solutions of pH 5.02, 7.00, 8.95, and 10.01. Figure 6b shows the response for the LIG–ISEs; a nonsignificant difference between the responses was observed for 1 mM ($p = 0.3487$) and 100 mM ($p = 0.4231$) nitrate concentration levels.

### Surface water analysis and sensor longevity

Samples from two lakes in Ames, IA were collected and tested according to US EPA method 9210a with the hydrophobic LIG–ISEs to validate the sensor performance in real samples. The LIG–ISEs were calibrated in the water samples and the emf response was monitored for 5 min in each sample. Results are comparable with an EPA–accepted analytical method performed by a secondary laboratory, as the concentrations are within the standard deviation of the LIG–ISE measurement. The LIG–ISEs were then stored in water samples for 5 weeks with calibration performed weekly to monitor the effect on the LOD and sensitivity, which demonstrate nonsignificant change on these performance parameters over a 3-week period; however, the sensors remain operational for up to 5 weeks. A statistically significant change in the sensitivity of the sensor was observed beyond week 3. This is a slightly shorter storage time compared to some nitrate ISEs, but these reports do not clarify storage and testing conditions or use unfeasible testing protocols for ISEs intended for in situ monitoring of nutrients (Table S2). SEM cross sectional images were also taken of freshly prepared LIG–ISEs, and those stored in water samples for 5 weeks (Fig. 7c and d, respectively). Membrane detachment can be seen clearly in the LIG–ISEs that were stored in surface water samples and could possibly explain the statistically significant change in membrane sensitivity observed after week 3 of storage. Further studies are investigating how to improve the LIG–ISE longevity to monitor nutrients in surface waters in situ.

## Conclusion

Higher temporal and spatial in situ monitoring of ions, particularly N, P, and K, would allow accurate and precise application of fertilizers reducing costs to farmers and offering researchers a tool to study nutrient run-off and the consequences associated with it. The present study explored implementing hydrophobic LIG fabricated via a double lasing process for monitoring ions in surface water samples. Nitrate was chosen as the ion of interest for this study due to the importance in fertilizer application, plant growth, and nutrient run-off research. The development of sufficiently selective anion selective membranes is still a challenge, and with the current platform, selectivity studies show notable interference from $Cl^-$, suggesting the possible necessity for desalinization in certain situations. Stability and longevity experiments displayed favorable results comparable to an EPA standard analytical method and demonstrate the potential applicability that hydrophobic LIG–ISEs have for low-cost long-term in situ monitoring of ions in water sources. The technique does not require post-fabrication annealing process nor the deposition of expensive metals to increase the electrical conductivity or electrocatalytic nature commonly used with other graphene-based sensors. The maskless lithography-free double lasing fabrication process, performed in an ambient environment, utilizes a laser commonly found in machine shops, demonstrating the feasibility of implementing a facile and scalable roll-to-roll manufacturing procedure for hydrophobic LIG. Future development of LIG–ISEs will focus increasing emf signal stability and work towards calibration-free sensors and the integration with wireless networks to perform long-term in-field studies. This could eventually lead to low-cost solid-contact ISEs for precision agriculture and surface water quality monitoring.

**Supplementary Information** The online version contains supplementary material available at https://doi.org/10.1007/s00604-022-05233-5.

**Funding** We gratefully acknowledge funding support from the National Institute of Food and Agriculture, U.S. Department of Agriculture, award numbers 2019–05855, 2020–04109, and 2018–672-67016–27578 awarded as a Center of Excellence. The National Science Foundation under award numbers CBET-1706994, CBET-1756999, CBET-1805512, ECCS-1841649, and CMMI-2037026. We also gratefully acknowledge Leigh Ann Long and the Water Quality Research Lab (WQRL) at Iowa State University for analyzing water samples.

## Declarations

**Conflict of interest** The authors declare no competing interests.

## References

1. Mirsky AE, Anson ML (1929) A description of the glass electrode and its use in measuring hydrogen ion concentration. J Biol Chem 81:581–587. https://doi.org/10.1016/s0021-9258(18)63713-5
2. Lindner E, Tóth K (2009) To the memory of Ernö Pungor: a subjective view on the history of ion-selective electrodes. Electroanalysis 21:1887–1894. https://doi.org/10.1002/elan.200904624
3. Srinivasan K, Rechnitz GA (1969) Selectivity studies on liquid membrane, ion-selective electrodes. Anal Chem 41:1203–1208. https://doi.org/10.1021/ac60279a014
4. Shao Y, Ying Y, Ping J (2020) Recent advances in solid-contact ion-selective electrodes: functional materials, transduction mechanisms, and development trends. Chem Soc Rev 49:4405–4465. https://doi.org/10.1039/c9cs00587k
5. Cattrall RW, Freiser H, Cattrall RW (1971) Coated wire ion selective electrodes. Anal Chem 43:1905–1906. https://doi.org/10.1021/ac60307a032

6. Michalska A (2012) All-solid-state ion selective and all-solid-state reference electrodes. Electroanalysis 24:1253–1265. https://doi.org/10.1002/elan.201200059
7. Kałuża D, Jaworska E, Mazur M et al (2019) Multiwalled carbon nanotubes-poly(3-octylthiophene-2,5-diyl) nanocomposite transducer for ion-selective electrodes: Raman spectroscopy insight into the transducer/membrane interface. Anal Chem 91:9010–9017. https://doi.org/10.1021/acs.analchem.9b01286
8. Guzinski M, Jarvis JM, Perez F et al (2017) PEDOT(PSS) as solid contact for ion-selective electrodes: the influence of the PEDOT(PSS) film thickness on the equilibration times. Anal Chem 89:3508–3516. https://doi.org/10.1021/acs.analchem.6b04625
9. Yin T, Qin W (2013) Applications of nanomaterials in potentiometric sensors. TrAC - Trends Anal Chem 51:79–86. https://doi.org/10.1016/j.trac.2013.06.009
10. Wallace GG, Chen J, Li D et al (2010) Nanostructured carbon electrodes. J Mater Chem 20:3553–3562. https://doi.org/10.1039/b918672g
11. Roy S, David-Pur M, Hanein Y (2017) Carbon nanotube-based ion selective sensors for wearable applications. ACS Appl Mater Interfaces 9:35169–35177. https://doi.org/10.1021/acsami.7b07346
12. Li F, Ye J, Zhou M et al (2012) All-solid-state potassium-selective electrode using graphene as the solid contact. Analyst 137:618–623. https://doi.org/10.1039/c1an15705a
13. Ping J, Wang Y, Ying Y, Wu J (2012) Application of electrochemically reduced graphene oxide on screen-printed ion-selective electrode. Anal Chem 84:3473–3479. https://doi.org/10.1021/ac203480z
14. Justino CIL, Gomes AR, Freitas AC et al (2017) Graphene based sensors and biosensors. TrAC - Trends Anal Chem 91:53–66. https://doi.org/10.1016/j.trac.2017.04.003
15. Lin J, Peng Z, Liu Y et al (2014) Laser-induced porous graphene films from commercial polymers. Nat Commun 5.https://doi.org/10.1038/ncomms6714
16. Kurra N, Jiang Q, Nayak P, Alshareef HN (2019) Laser-derived graphene: a three-dimensional printed graphene electrode and its emerging applications. Nano Today 24:81–102
17. Stanford MG, Zhang C, Fowlkes JD et al (2020) High-resolution laser-induced graphene. Flexible electronics beyond the visible limit. ACS Appl Mater Interfaces 12:10902–10907. https://doi.org/10.1021/acsami.0c01377
18. Chyan Y, Ye R, Li Y et al (2018) Laser-induced graphene by multiple lasing: toward electronics on cloth, paper, and food. ACS Nano 12:2176–2183. https://doi.org/10.1021/acsnano.7b08539
19. Secor EB, Prabhumirashi PL, Puntambekar K et al (2013) Inkjet printing of high conductivity, flexible graphene patterns. J Phys Chem Lett 4:1347–1351. https://doi.org/10.1021/jz400644c
20. Parate K, Rangnekar SV, Jing D et al (2020) Aerosol-jet-printed graphene immunosensor for label-free cytokine monitoring in serum. ACS Appl Mater Interfaces 12:8592–8603. https://doi.org/10.1021/acsami.9b22183
21. Jin Z, McNicholas TP, Shih CJ et al (2011) Click chemistry on solution-dispersed graphene and monolayer CVD graphene. Chem Mater 23:3362–3370. https://doi.org/10.1021/cm201131v
22. Soares RRA, Hjort RG, Pola CC et al (2020) Laser-induced graphene electrochemical immunosensors for rapid and label-free monitoring of salmonella enterica in chicken broth. ACS Sensors. https://doi.org/10.1021/acssensors.9b02345
23. Yagati AK, Behrent A, Beck S et al (2020) Laser-induced graphene interdigitated electrodes for label-free or nanolabel-enhanced highly sensitive capacitive aptamer-based biosensors. Biosens Bioelectron 164:112272. https://doi.org/10.1016/j.bios.2020.112272
24. Yang Y, Song Y, Bo X et al (2020) A laser-engraved wearable sensor for sensitive detection of uric acid and tyrosine in sweat. Nat Biotechnol 38:217–224. https://doi.org/10.1038/s41587-019-0321-x
25. Torrente-Rodríguez RM, Tu J, Yang Y et al (2020) Investigation of cortisol dynamics in human sweat using a graphene-based wireless mhealth system. Matter 2:921–937. https://doi.org/10.1016/j.matt.2020.01.021
26. Cardoso AR, Marques AC, Santos L et al (2019) Molecularly-imprinted chloramphenicol sensor with laser-induced graphene electrodes. Biosens Bioelectron 124–125:167–175. https://doi.org/10.1016/j.bios.2018.10.015
27. Garland NT, McLamore ES, Cavallaro ND et al (2018) Flexible laser-induced graphene for nitrogen sensing in soil. ACS Appl Mater Interfaces 10:39124–39133. https://doi.org/10.1021/acsami.8b10991
28. Kucherenko IS, Sanborn D, Chen B et al (2020) Ion-selective sensors based on laser-induced graphene for evaluating human hydration levels using urine samples. Adv Mater Technol 5:1–9. https://doi.org/10.1002/admt.201901037
29. Bauer M, Wunderlich L, Weinzierl F et al (2020) Electrochemical multi-analyte point-of-care perspiration sensors using on-chip three-dimensional graphene electrodes. Anal Bioanal Chem. https://doi.org/10.1007/s00216-020-02939-4
30. Umezawa Y, Bühlmann P, Umezawa K et al (2000) Potentiometric selectivity coefficients of ion-selective electrodes part I. Inorganic cations (technical report). Pure Appl Chem 72:1851–2082. https://doi.org/10.1351/pac200072101851
31. Fibbioli M, Morf WE, Badertscher M et al (2000) Potential drifts of solid-contacted ion-selective electrodes due to zero-current ion fluxes through the sensor membrane. Electroanalysis 12:1286–1292. https://doi.org/10.1002/1521-4109(200011)12:16<1286::AID-ELAN1286>3.0.CO;2-Q
32. Inagaki M, Ibuki T, Takeichi T (1992) Carbonization behavior of polyimide films with various chemical structures. J Appl Polym Sci 44:521–525. https://doi.org/10.1002/app.1992.070440316
33. Ni Z, Wang Y, Yu T, Shen Z (2008) Raman spectroscopy and imaging of graphene. Nano Res 1:273–291. https://doi.org/10.1007/s12274-008-8036-1
34. Pimenta MA, Dresselhaus G, Dresselhaus MS et al (2007) Studying disorder in graphite-based systems by Raman spectroscopy. Phys Chem Chem Phys 9:1276–1291. https://doi.org/10.1039/b613962k
35. Nguyen VT, Le HD, Nguyen VC et al (2013) Synthesis of multilayer graphene films on copper tape by atmospheric pressure chemical vapor deposition method. Adv Nat Sci Nanosci Nanotechnol 4:2–7. https://doi.org/10.1088/2043-6262/4/3/035012
36. He N, Papp S, Lindfors T et al (2017) Pre-polarized hydrophobic conducting polymer solid-contact ion-selective electrodes with improved potential reproducibility. Anal Chem 89:2598–2605. https://doi.org/10.1021/acs.analchem.6b04885
37. Lamour G, Hamraoui A, Buvailo A et al (2010) Contact angle measurements using a simplified experimental setup. J Chem Educ 87:1403–1407. https://doi.org/10.1021/ed100468u
38. De Gennes PG (1985) Wetting: statics and dynamics. Rev Mod Phys 57:827–863. https://doi.org/10.1103/RevModPhys.57.827
39. Vazquez G, Alvarez E, Navaza JM (1995) Surface tension of alcohol + water from 20 to 50 °C. J Chem Eng Data 40:611–614. https://doi.org/10.1021/je00019a016
40. Bühlmann P, Chen LD (2012) Ion-selective electrodes with ionophore-doped sensing membranes. In: Gale PA, Steed JW (eds) Supramolecular Chemistry, 1st ed. Wiley, New York
41. Lindner E, Gyurcsányi RE (2009) Quality control criteria for solid-contact, solvent polymeric membrane ion-selective

electrodes. J Solid State Electrochem 13:51–68. https://doi.org/10.1007/s10008-008-0608-1
42. Crespo GA, Macho S, Bobacka J, Rius-Ruiz FX (2009) Transduction mechanism of carbon nanotubes in solid-contact ion-selective electrodes Gasto´n. J Solid State Electrochem 81:676–681. https://doi.org/10.1007/s10008-008-0579-2
43. Kim HJ, Sudduth KA, Hummel JW (2009) Soil macronutrient sensing for precision agriculture. J Environ Monit 11:1810–1824. https://doi.org/10.1039/b906634a
44. Lin PKT, Araujo AN, Montenegro MCBSM, Pérez-Olmos R (2005) New PVC nitrate-selective electrode: application to vegetables and mineral waters. J Agric Food Chem 53:211–215. https://doi.org/10.1021/jf049227u
45. Minero C, Chiron S, Falletti G et al (2007) Photochemincal processes involving nitrite in surface water samples. Aquat Sci 69:71–85. https://doi.org/10.1007/s00027-007-0881-6
46. Cuartero M, Crespo GA, Bakker E (2015) Tandem electrochemical desalination-potentiometric nitrate sensing for seawater analysis. Anal Chem 87:8084–8089. https://doi.org/10.1021/acs.analchem.5b01973
47. Radu A, Anastasova-Ivanova S, Paczosa-Bator B et al (2010) Diagnostic of functionality of polymer membrane - based ion selective electrodes by impedance spectroscopy. Anal Methods 2:1490–1498. https://doi.org/10.1039/c0ay00249f
48. Joon NK, He N, Ruzgas T et al (2019) PVC-based ion-selective electrodes with a silicone rubber outer coating with improved analytical performance. Anal Chem 91:10524–10531. https://doi.org/10.1021/acs.analchem.9b01490
49. Sundfors F, Lindfors T, Höfler L et al (2009) FTIR-ATR study of water uptake and diffusion through ion-selective membranes based on poly(acrylates) and silicone rubber. Anal Chem 81:5925–5934. https://doi.org/10.1021/ac900727w
50. Lindfors T, Sundfors F, Höfler L, Gyurcsányi RE (2009) FTIR-ATR study of water uptake and diffusion through ion-selective membranes based on plasticized poly(vinyl chloride). Electroanalysis 21:1914–1922. https://doi.org/10.1002/elan.200904609
51. Griffiths K, Dale C, Hedley J et al (2014) Laser-scribed graphene presents an opportunity to print a new generation of disposable electrochemical sensors. Nanoscale 6:13613–13622. https://doi.org/10.1039/c4nr04221b
52. Li B, Fan Y, Huang Y et al (2020) Toward long-term accurate and continuous monitoring of nitrate in wastewater using poly (tetrafluoroethylene) (PTFE)−solid-state ion-selective electrodes (S-ISEs). ACS Sensors 5:3182–3193. https://doi.org/10.1021/acssensors.0c01422
53. Hu J, Stein A, Bühlmann P (2016) Rational design of all-solid-state ion-selective electrodes and reference electrodes. TrAC - Trends Anal Chem 76:102–114. https://doi.org/10.1016/j.trac.2015.11.004
54. Bobacka J (1999) Potential stability of all-solid-state ion-selective electrodes using conducting polymers as ion-to-electron transducers. Anal Chem 71:4932–4937. https://doi.org/10.1021/ac990497z
55. Ping J, Wang Y, Wu J, Ying Y (2011) Development of an all-solid-state potassium ion-selective electrode using grapheme as the solid-contact transducer. Electrochem commun 13:1529–1532. https://doi.org/10.1016/j.elecom.2011.10.018
56. Hu J, Zou XU, Stein A, Bühlmann P (2014) Ion-selective electrodes with colloid-imprinted mesoporous carbon as solid contact. Anal Chem 86:7111–7118. https://doi.org/10.1021/ac501633r
57. Paczosa-Bator B, Cabaj L, Piech R, Skupień K (2013) Potentiometric sensors with carbon black supporting platinum nanoparticles. Anal Chem 85:10255–10261. https://doi.org/10.1021/ac402885y
58. Rousseau CR, Bühlmann P (2021) Calibration-free potentiometric sensing with solid-contact ion-selective electrodes. TrAC - Trends Anal Chem 140:116277. https://doi.org/10.1016/j.trac.2021.116277
59. Teresa M, Vasconcelos SD, Machado AASC (1988) Effect of temperature on the response characteristics of ion-selective electrodes based on solid silver salts applied to electrically conductive epoxy supports. Analyst 113:49–55. https://doi.org/10.1039/AN9881300049
60. Han JH, Cui G, Kim SJ et al (2001) Effect of dissolved CO2 on the potential stability of all-solid-state ion-selective electrodes. Analyst 126:2040–2043. https://doi.org/10.1039/b105585m
61. Dutta S, Sarma D, Nath P (2015) Ground and river water quality monitoring using a smartphone-based pH sensor. AIP Adv 5.https://doi.org/10.1063/1.4921835